

# MODELING AND PROGRESSIVE DAMAGE ANALYSIS OF FRP LAMINATES WITH PERIDYNAMIC THEORY

Y. L. Hu, Y. Yu\*, H. Wang

School of Aeronautics and Astronautics, Shanghai Jiao Tong University, Shanghai, China

\* Y. Yu ([yuyin@sjtu.edu.cn](mailto:yuyin@sjtu.edu.cn))

**Keywords:** *peridynamic; progressive damage; fiber-reinforced composite laminates; modeling; GPU computing*

## 1. Introduction

In the last decade, the usage of composite materials on long-range, wide-body jet airliners such as Airbus A350 and Boeing 787 have rapidly increased to about half of the total weight. Moreover, the application of composite materials is moving from lightly-loaded secondary structures to highly-loaded primary elements such as fuselage and wings. In order to confront the challenges brought by the expansions of usage and application, various numerical methods, especially the Finite Element (FE) methods, have been developed to predict the performance and analyze the progressive damages of composite structures. Although many FE models can provide high accuracy in analyzing composites, they still have limitations in dealing with discontinuities such as damages, fractures, crack propagations, delaminations and penetrations. This is due to the essence of conventional FE method is partial differential equations of the displacement field based upon continuous mechanical system, whereas it is quite difficult to get the derivatives of displacement in these discontinuous areas. As a result, traditional FE methods often suffer from the difficulties in solving discontinuous problems of composite structures [1-2].

Recently, a novel solid mechanics theory, *Peridynamic Theory*, has been proposed by Silling [3] to overcome the numerical difficulties because of discontinuities. Peridynamic theory employs integration rather than differentiation in its motion equation so that it can avoid calculating the derivatives of displacement in discontinuous areas. Due to this feature, peridynamic method is more appropriate than FE method in analyzing the discontinuous problems. Peridynamic theory takes nonlocal interactions into consideration and uses so called *bonds* to describe the internal forces between particles. When damages emerge in materials or structures, bonds in these damaged areas will permanently break and cause a decline in load-carrying capacity of the structure. Moreover, there is

no necessity to use additional failure criteria or crack growth laws because the constitutive information of materials can be included in the peridynamic motion equation. Damages and failures can occur freely and spontaneously in the model.

The investigations on composite structures with peridynamic theory are becoming one of the most important branches. With the aid of a peridynamic analysis program EMU, Sandia lab [4], Askari [5] has predicted the failure modes and ultimate strength of center-notched laminates under a tensile loading with 2D and 3D models. Xu [6-7] has analyzed the mechanics responses of composite laminates under low velocity impact and hailstone impact, and obtained the delamination patterns, areas and residual strength under different impact energy. Kilic [8-9] considers the inhomogeneous nature of composites as a necessary fact in laminate modeling, and separates the model into fiber and matrix subregions, thus, his model can reflect the influence of fiber volume fraction. Hu [10] has established an unidirectional laminate model and analyzed the dynamic loading effect on the damages of brittle materials.

Among these works on composite structures, only few kinds of bonds are used to define the interactions in composites, however, the fiber reinforced composite possesses many complex anisotropic behaviors which need to be described by more types of bonds with distinct performances. In this paper, a new 3D peridynamic laminate model for fiber-reinforced composite laminates is proposed and applied to simulate the progressive damages and failures in laminates with notch. In order to improve the depiction of composite's anisotropy, this approach introduces various types of *bonds* to define the laminate's properties in different directions. Concept of off-axial modulus in classic laminate theory is employed into the bonds' definition. The properties of bonds, such as *micromodulus* and *critical stretch*, are deduced from the parameters in elasticity and composite mechanics. Based on this peridynamic laminate model, progressive damages

and failures in notched laminates with different stacking sequences are analyzed under tensile loading. The numerical predictions have good agreements with results from the literatures and experiments.

## 2. Peridynamic Theory

Peridynamic theory [3] hypothesizes that an object possesses a reference configuration  $R$  where each particle  $\mathbf{x}$  owns a subregion  $R^0$  with a radius  $\delta$ , as presented in Fig.1. Such a number  $\delta$  is called the *material horizon*. Particle  $\mathbf{x}$  interacts with the rest particles  $\mathbf{x}'$  in subregion  $R^0$  through a vector-valued function  $\mathbf{f}$  which is called the *pairwise force function*, a function with a dimension of force per unit volume squared. At any time  $t$ , the equation of motion in peridynamic theory can be written as

$$\rho \ddot{\mathbf{u}}(\mathbf{x}, t) = \mathbf{L}(\mathbf{x}, t) + \mathbf{b}(\mathbf{x}, t) \quad (1)$$

where  $\rho$  is the density of material,  $\mathbf{u}$  is the displacement vector,  $\mathbf{b}$  is the external body force density,  $\mathbf{L}$  is the internal body force density.

$$\mathbf{L}(\mathbf{x}, t) = \int_{R^0} \mathbf{f}(\boldsymbol{\eta}, \boldsymbol{\xi}) dV_{\mathbf{x}'} \quad \forall \mathbf{x} \in R, t \geq 0 \quad (2)$$

where  $\boldsymbol{\eta} = \mathbf{u}' - \mathbf{u}$ ,  $\boldsymbol{\xi} = \mathbf{x}' - \mathbf{x}$  are relative displacement vectors and relative position vectors of the pair of particles in the reference configuration,  $V_{\mathbf{x}'}$  is the volume of particle  $\mathbf{x}'$ . Thus, the relative position vectors between  $\mathbf{x}$  and  $\mathbf{x}'$  in the deformed configuration can be written as  $\boldsymbol{\eta} + \boldsymbol{\zeta}$ , and the distance between two particles can be written as  $y = |\boldsymbol{\eta} + \boldsymbol{\zeta}|$  correspondingly.

As for a *microelastic* material, its pairwise force function can be written as [11]

$$\mathbf{f}(\boldsymbol{\eta}, \boldsymbol{\xi}) = \frac{\boldsymbol{\xi} + \boldsymbol{\eta}}{|\boldsymbol{\xi} + \boldsymbol{\eta}|} f(y, \boldsymbol{\xi}) \quad \forall \boldsymbol{\eta}, \boldsymbol{\xi} \quad (3)$$

Where  $f(y, \boldsymbol{\xi})$  is a scalar-valued function contains all constitutive information and failure definitions of the material. The scalar-valued function  $f$  is depended on the relative position and distance between particle  $\mathbf{x}$  and  $\mathbf{x}'$ . Pairwise force function of brittle materials is defined as

$$\mathbf{f}(\boldsymbol{\eta}, \boldsymbol{\xi}) = \frac{\boldsymbol{\xi} + \boldsymbol{\eta}}{|\boldsymbol{\xi} + \boldsymbol{\eta}|} \mu(\boldsymbol{\xi}, t) cs \quad (4)$$

where  $s$  is the *bond stretch* presenting the relative elongation

$$s = \frac{|\boldsymbol{\xi} + \boldsymbol{\eta}| - |\boldsymbol{\xi}|}{|\boldsymbol{\xi}|} = \frac{y - |\boldsymbol{\xi}|}{|\boldsymbol{\xi}|} \quad (5)$$

In order to describe fracture of the bonds, a time-dependent function  $\mu$  is introduced [11]

$$\mu(\boldsymbol{\xi}, t) = \begin{cases} 1 & \text{if } s(t', \boldsymbol{\xi}) < s_0 \\ 0 & \text{otherwise} \end{cases} \quad t' \in (0, t) \quad (6)$$

where  $s_0$  is the *critical stretch* indicating a critical value which causes permanent breaking and decline in the load-carrying capacity of bonds. According to the definition of bonds' fracture, the damage of a particle  $\mathbf{x}$  at some time  $t$  can be defined as

$$\phi(\mathbf{x}, t) = 1 - \frac{\int_R \mu(\boldsymbol{\xi}, t) dV_{\mathbf{x}'}}{\int_R dV_{\mathbf{x}'}} \quad (7)$$

It has been showed by equations (4) to (6) that all descriptions of damage or fracture are included in the definition of pairwise force function and there is no necessity to use additional criterion of strength, stress intensity factors or crack propagation regulations to assist the solutions.

## 3. Laminate Modeling

In the above pairwise force function, there are two variables to be defined: *micromodulus*  $c$  and *critical stretch*  $s_0$ . Due to the distinction between composites and other materials, these values should be deduced according to composite's characteristics which are illustrated in this section. This model of fiber reinforced composite laminates is homogenously discretized into cubic lattice grids. In addition, the calculation model is based on a simple assumption for out plane direction that the range of subregion can only extend to the adjacent layers, as presented in Fig.2.

### 3.1 Micromodulus

Fiber reinforced composites are inherent anisotropic, they have excellent performances along the fiber orientation (longitudinal direction), but weak properties in the direction perpendicular to the fiber orientation (transverse direction). As a result, *micromodulus* of the bonds in longitudinal region and transverse region are defined in separate ways. Suppose that the bonds, whose orientations are in the same direction of fibers, afford the longitudinal stiffness of the laminate, while the others constitute the transverse stiffness. As a result, the subregion of a node will be divided into longitudinal region and transverse region (Fig.3). A further classification is that in the longitudinal region, the in-plane and interlayer bonds are respectively defined as *fiber bonds* and *longitudinal interlayer bonds* respectively. Similarly, the in-plane and interlayer bonds in the transverse region are defined as *matrix bonds* and *transverse interlayer bonds*. Among these bonds,

micromodulus of fiber and interlayer bonds are independent on their orientations, but micromodulus of matrix bonds are varied by the included angle between bond and fiber orientation according to the off-axial modulus in classic laminate theory. In addition, the performances of all bonds are related to their length, it can be summarized that the shorter a bond's length is, the stronger the interactive connection becomes. Micromodulus of bonds in longitudinal region is defined as

$$c_{\text{longitudinal}} = e^{-\left(\frac{|\xi|}{\delta}\right)} \frac{Q_L}{Q_{11}} \bar{c}_L \quad (8)$$

$$Q_L = \begin{cases} Q_{11} & \text{in-plane bonds} \\ Q_{\text{layer}} & \text{interlayer bonds} \end{cases}$$

And micromodulus of the bonds in transverse region is stated as

$$c_{\text{transverse}} = e^{-\left(\frac{|\xi|}{\delta}\right)} \frac{Q_T}{Q_{22}} \bar{c}_T \quad (9)$$

$$Q_T = \begin{cases} \bar{Q}_\alpha & \text{in-plane bonds} \\ Q_{\text{layer}} & \text{interlayer bonds} \end{cases}$$

where  $\bar{Q}_\alpha$  is the off-axial stiffness of composite mechanics,  $\alpha$  is the included angle between bond and fiber orientation.

$$\bar{Q}_\alpha = Q_{11} \cos^4 \alpha + 2(Q_{12} + 2Q_{66}) \sin^2 \alpha \cos^2 \alpha + Q_{22} \sin^4 \alpha \quad (10)$$

where  $Q_{11}$ ,  $Q_{22}$  are the stiffness of the lamina in the longitudinal and transverse direction,  $Q_{12}$ ,  $Q_{66}$  represent the in-plane coupling stiffness and shear stiffness.

Considering a  $[0]_n$  unidirectional laminate under a longitudinal load, it will produce a homogeneous strain  $\varepsilon$  along the loading direction. The internal force on an arbitrary cross section of a laminate is constituted by forces of all bonds through that cross section, and it should be numerically equal to the result of conventional mechanics theories.

$$\sum_{i \in R^+} \sum_{j \in R^-} e^{-\left(\frac{|\xi_{ij}|}{\delta}\right)} \frac{Q_{ij}}{Q_{11}} \bar{c}_L s \cos^2 \alpha_{ij} V_j V_i = Q_{11} \varepsilon A \quad (11)$$

where  $A$  presents the area of the cross section, the subscript  $ij$  indicates the bonds connecting node  $i$  in region  $R^+$  and node  $j$  in region  $R^-$  and  $Q_{ij}$  illustrates the stiffness mentioned in equation(8,9). Due to the uniform discretization, all nodes are provided with the same volume  $V_{\text{node}} = V_i = V_j$ , and the bond stretch  $s$  is approximately equivalent to strain  $\varepsilon$  when

the homogeneous deformation maintains a relatively low value. Hence,

$$\bar{c}_L = \frac{Q_{11}}{\lambda_L \cdot \Delta x \cdot V_{\text{node}}} \quad (12)$$

where  $\Delta x$  is the mesh spacing,  $\lambda_L$  equals to

$$\lambda_L = \sum_{i \in R^+} \sum_{j \in R^-} e^{-\left(\frac{|\xi_{ij}|}{\delta}\right)} \frac{Q_{ij}}{Q_{11}} \cos^2 \alpha_{ij} \quad (13)$$

Therefore, the micromodulus of fiber bonds and longitudinal interlayer bonds can be written as

$$c_{\text{fiber}}, c_{\text{longitudinal interlayer}} = e^{-\left(\frac{|\xi|}{\delta}\right)} \frac{Q_L}{\lambda_L \cdot \Delta x \cdot V_{\text{node}}} \quad (14)$$

Similarly, when the laminate is under a transverse loading

$$\sum_{i \in R^+} \sum_{j \in R^-} e^{-\left(\frac{|\xi_{ij}|}{\delta}\right)} \frac{Q_{ij}}{Q_{22}} \bar{c}_T s \cos^2 \alpha_{ij} V_j V_i = Q_{22} \varepsilon A \quad (15)$$

The micromodulus  $c$  of matrix bonds and transverse interlayer bonds can be deduced by combining equations (9) and (15).

$$c_{\text{matrix}}, c_{\text{transverse interlayer}} = e^{-\left(\frac{|\xi|}{\delta}\right)} \frac{Q_T}{\lambda_T \cdot \Delta x \cdot V_{\text{node}}} \quad (16)$$

### 3.2 Critical Stretch

The critical stretch  $s_0$  describes the elongation of bond and has the same form with traditional strains in mechanics theory so that maximum strains are used to denote critical stretches. Since the fiber reinforced composites afford distinct strengths in different directions, the critical stretches  $s_0$  are also set with different values in this approach.

$$\begin{cases} s_0^{\text{ft}} = \frac{X^T}{E_{11}}, s \geq 0 & \text{fiber bonds} \\ s_0^{\text{fc}} = \frac{X^C}{E_{11}}, s < 0 & \text{fiber bonds} \\ s_0^{\text{mt}} = \frac{Y^T}{E_{22}}, s \geq 0 & \text{matrix and interlayer bonds} \\ s_0^{\text{mc}} = \frac{Y^C}{E_{22}}, s < 0 & \text{matrix and interlayer bonds} \end{cases} \quad (17)$$

When bonds are subjected to a tensile loading, brittle fracture will occur when their stretches reach the critical value, rendering to an abrupt decline in bond's load-carrying capability. As far as compressive loading is concerned, the bonds' performances are slightly different. When fiber bonds collapse, they sustain no force either, but the

matrix and interlayer bonds still have some capacity in carrying load because matrix materials cannot cross over each other. Matrix, interlayer bonds are assumed to remain half performance after their stretches exceed the compressive critical value.

#### 4. Numerical Implementation

In the numerical implementation, the reference configuration is uniformly discretized into vast number of nodes and the integration in equation (2) can be replaced by a finite sum

$$\rho \ddot{\mathbf{u}}_i^n = \sum_p \mathbf{f}(\mathbf{u}_p^n - \mathbf{u}_i^n, \mathbf{x}_p - \mathbf{x}_i) V_i + \mathbf{b}_i^n \quad (18)$$

where the sum range is within the material horizon, the superscript  $n$  indicates the number of time step, and the subscript  $i$  represents node number.

The numerical method of peridynamic theory is quite computational expensive, a common defect among most meshless methods, as a result of substantial quantity of bonds is involved in the computing. Fortunately, the node displacement possesses an explicit calculation formula which implies a high parallelism. Thus, the GPU parallel computing technology [12-15] is utilized in this approach to improve calculation efficiency.

#### 5. Numerical Prediction and Experimental Verification

In this section, unidirectional laminates and a quasi-isotropic laminate are successively analyzed to simulate the progressive damage and failure in laminates.

##### 5.1 Prediction Model

For the unidirectional laminate, the dimension is 504mm in length, 127mm in width and 2mm in thickness. Its layups are  $[0]_8$ ,  $[45]_8$ , and  $[90]_8$  and contains a 25.4mm×6.35 mm's notch in the center as indicated in Fig.4.

For the quasi-isotropic laminate, the dimension is set up according to the requirement in ASTM D5766 [16]. Its layup is  $[45/0/-45/90]_s$  and the laminate has an open hole with a 6mm diameter in the center.

Both of the unidirectional and quasi-isotropic laminates are fixed on one side and exerted by a tensile loading on the other side, the boundary conditions are set onto the nodes within 3 grid spacing from the ends. The properties of T700/977 carbon-epoxy composite are assigned to the lamina. The thickness of a single ply is 0.25mm, material density is 1580kg/m<sup>3</sup>, longitudinal Young's modulus  $E_{11}$ =142.1GPa, transverse Young's modulus

$E_{22}$ =8.73GPa, shear modulus  $G_{12}$ =4.49GPa, principal Poisson's ratio  $\nu_{12}$ =0.33, longitudinal tensile strength  $X^T$ =2.668GPa, longitudinal compressive strength  $X^C$ =1.488GPa, transverse tensile strength  $Y^T$ =91.8MPa and transverse compressive strength  $Y^C$ =291MPa.

##### 5.2 Analysis of Unidirectional Laminates

When the displacement of the loading end is relatively small, implying that damages and failures have not occurred in the laminates, the deformation of unidirectional laminates shows great agreement with the FE results as illustrated in Fig.5. Fig.5(a), Fig.5(c) and Fig.5(e) is FEM results of  $[0]_8$ ,  $[45]_8$  and  $[90]_8$  laminates; Fig.5(b), Fig.5(d) and Fig.5(f) are their peridynamic results. The geometrical discontinuities induced by a center notch influence the displacement contours around its boundary, which reflects the distribution of internal forces in the laminates. Due to the refined anisotropic definitions introduced in this model, it can be seen that the displacement contours have different patterns with the rotation of fiber orientations and they correlate well with each other.

With the augment of loading, the concentration of internal force induces the initial damages on the notch boundary. Cracks initiate from the edge of notch and tips extend along different directions which are compatible with the ply orientations, as Fig.6 to Fig.8 presents. Predicted results indicate that local matrix fracture on the edge of the center notch usually emerges before the occurrence of other kinds of damages. The initial matrix failures trigger the onset of cracks and make the cracks spreading along fiber directions. Several results of different steps are chosen to illustrate the process of crack growth in unidirectional laminates. Fig.6 shows the crack propagations in  $[0]_8$  laminate, the spectrum denotes the damage extent, 0.0 means no damage and 1.0 represents totally damaged. Crack initiates from the notch's edge and its tips extend along the fiber direction as the loading increases. Since the matrix bonds own much weaker properties than the fiber bonds, it is reasonable to observe that matrix failure is the foremost failure mode appeared during the crack initiating phase. Similar traits of crack growth are also found in the  $[90]_8$  laminate which is illustrated in Fig.7. As the  $[90]_8$  laminate is loaded in the transverse direction, the matrix bonds still dominate the load-carrying capacity so that matrix splitting occurs before fiber fractures. Crack growth is also influenced by the fiber orientation, expanding straightly forward until the crack tip reaches the

lateral sides. Both of the simulation results of crack propagation in  $[0]_8$  and  $[90]_8$  unidirectional laminates are same to those results predicted in the literatures [8-9] and obtained from experiments [17]. The crack propagating direction of  $[45]_8$  laminate, however, does not spread along the  $45^\circ$  direction, it shows a deviation towards the  $90^\circ$  direction, as presented in Fig.8. This may due to the high speed loading, because it will introduce a high strain rate which has a significant effect on material response. Under a high speed loading, the maximum normal stress is much higher than that of static loading [18], which enables a possibility for composites to split along the transverse direction. Both of the  $[45]_8$  and  $[90]_8$  unidirectional laminates are finally fractured by the matrix splitting, however, the  $[0]_8$  unidirectional laminate is failed because of fiber break on the loading ends which are identical to the results of Askari [5].

### 5.3 Analysis of Quasi-isotropic Laminate

The quasi-isotropic laminate was tested on a MTS machine and an optical instrument was used to get the full-field displacement contour around the circular hole. The test sample was printed with speckle patterns on the surface which was measured by the digital cameras.

Fig.9 shows that the analysis gives correct elastic deformation around the circle hole and excellently agrees with the results of Digital Image Correlation (DIC). Fig.9(a) and Fig.9(c) denote the longitudinal and transverse deformations on the superficial  $45^\circ$  layer when the displacement on the loading side reaches 0.3mm, which is a safe value ensuring that there will be no damage produced in laminates. From Fig.9(b), it can be seen that the maximum and minimum value of longitudinal displacement are 0.1751mm and 0.1338mm respectively, it compares well with the numerical predictions which is 0.1856mm and 0.1234mm respectively. Their relative errors are 5.99% and 7.77% separately. The numerical analysis shows a symmetrical pattern (Fig.9(c)) for transverse displacement, while, the measurement result contains a slight slope (Fig.9(d)). It is caused by inevitable tolerances and gaps in the configuration of test machines, which produced a minute transverse rigid body displacement. It can be verified by the asymmetric spectrum limitations of Fig.9(d) which contains a little deviation in the transverse direction. In general, Fig.9 shows an identical tendency in longitudinal and transverse elastic deformations and

a good numerical agreement between peridynamic and experimental results.

As the load increases, damages begin to emerge on the edge and then disseminate to surrounding areas as presented in Fig.10. Since the stack sequence is symmetrical, the numerical analysis has obtained symmetric results on layers in the lower half, so that only the upper half of the laminate is showed in this picture. Predictions of the in-plane failure in each layer and delamination in the interlayer during the progressive damage process are illustrated in Fig.10. From the in-plane damages results, it can be seen that at the very beginning of crack initiation, matrix splits are parallel to the ply orientation which is consistent to the phenomenon observed from unidirectional laminates. Whereas, as the load rises, crack growth no longer spreads along the fiber direction, instead, it starts to spread rapidly in the transverse direction. The final failure mode of in-plane results shows that the outer  $45^\circ$  layer receives more severe damages than other layers and there are matrix splits along the ply orientation.

As presented in Fig.10, interlayer damages are able to be observed simultaneously via using this peridynamic approach. Similar to the inequity of in-plane damages, the outer interlayer comprises more serious damages than the inner ones. It can be seen that the interlamination between  $45^\circ$  and  $0^\circ$  layers has received the maximum damage in terms of extent and coverage. This inequity of damage in interlayer damage may mainly due to the outer layers' lack of lateral supports, and it is vulnerable to the out plane forces existed in the transient moment when fracture happens.

Finally, the ultimate failure mode of the laminate will be obtained by stacking these layers and interlaminations collectively, as indicated in Fig.11. The test result shows that the outer  $45^\circ$  layer contains more severe damages than the inside layers and the matrix splits along the ply orientation. The experiment result verifies that this approach can give correct predictions to laminate's deformation and failure. Generally, it is not easy for conventional FE methods to get such complex and detailed patterns for in-plane and interlayer damages synchronously.

### 6. Conclusion

Introduction of the off-axial modulus into bond definition is able to give a refined description of anisotropic behaviors of composites. Various types of bonds are employed in this approach and its predictions agree well with results from the literatures and experiments.

This approach provides no difficulties in analyzing damage propagation in discontinuous areas, and can propose novel views of failures which are figured by particles instead of elements. More detailed and complex process of damage propagations for composite materials can be exposed by this approach. Therefore, this approach is quite appropriate for structural analysis of composite materials.

### Figures

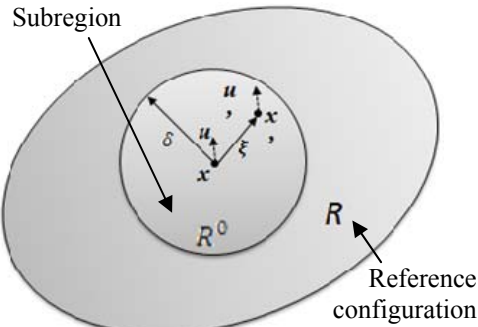


Fig.1 Peridynamic model

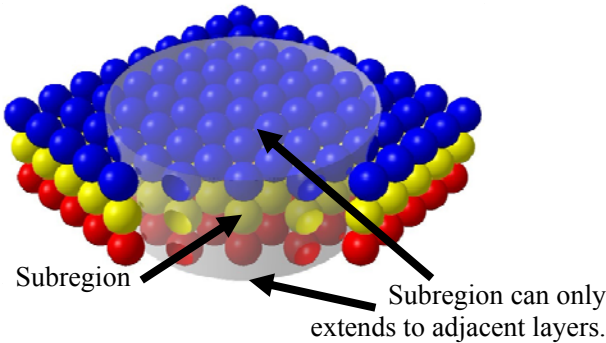


Fig.2 Limitation of composite material's subregion

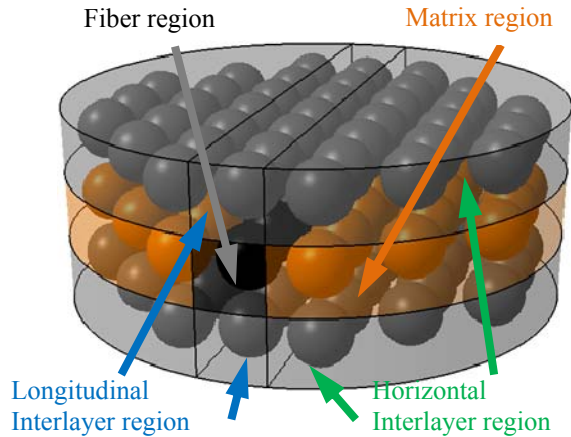


Fig.3 Division of a subregion

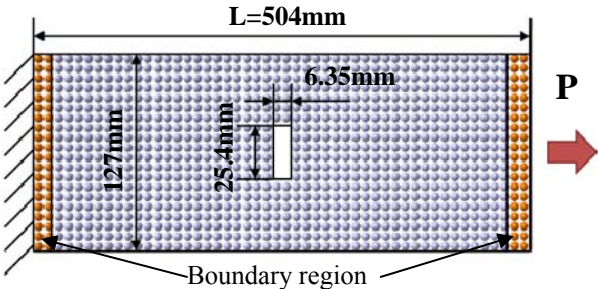


Fig.4 Prediction model of notched laminate

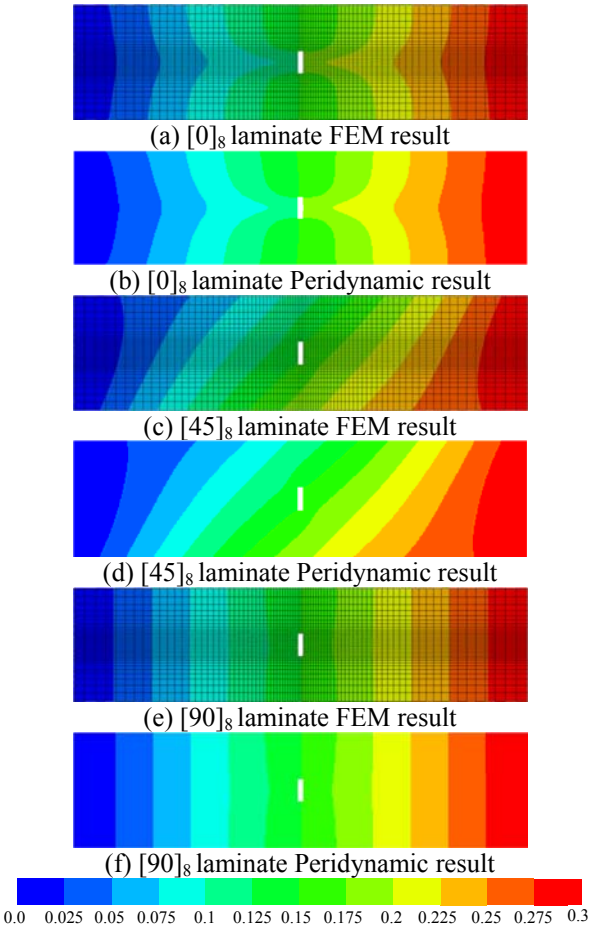


Fig.5 Elastic deformation of unidirectional laminates

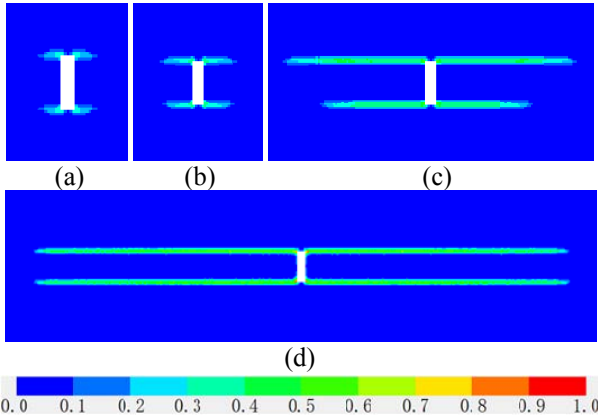


Fig.6 Matrix cracks in [0]<sub>8</sub> laminates

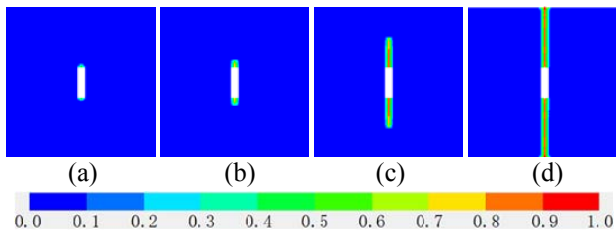


Fig.7 Matrix cracks in  $[90]_8$  laminates

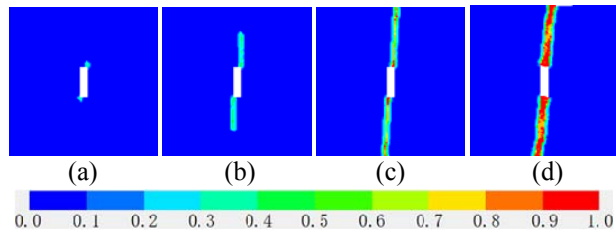


Fig.8 Matrix cracks in  $[45]_8$  laminates

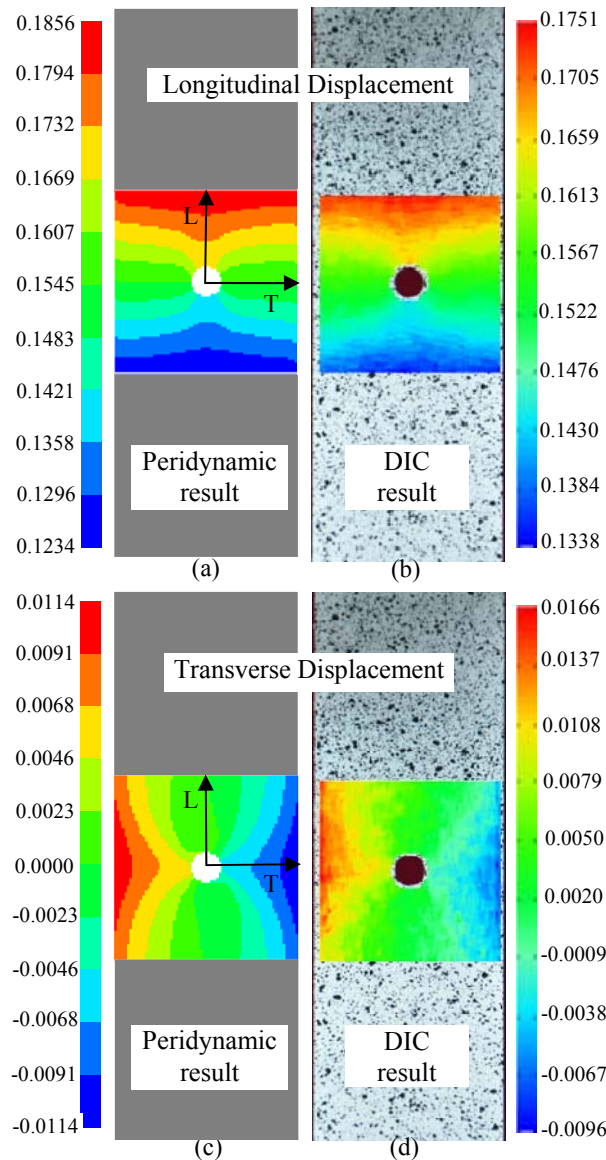


Fig.9 Comparison of the displacement around the open hole (Unit: mm)

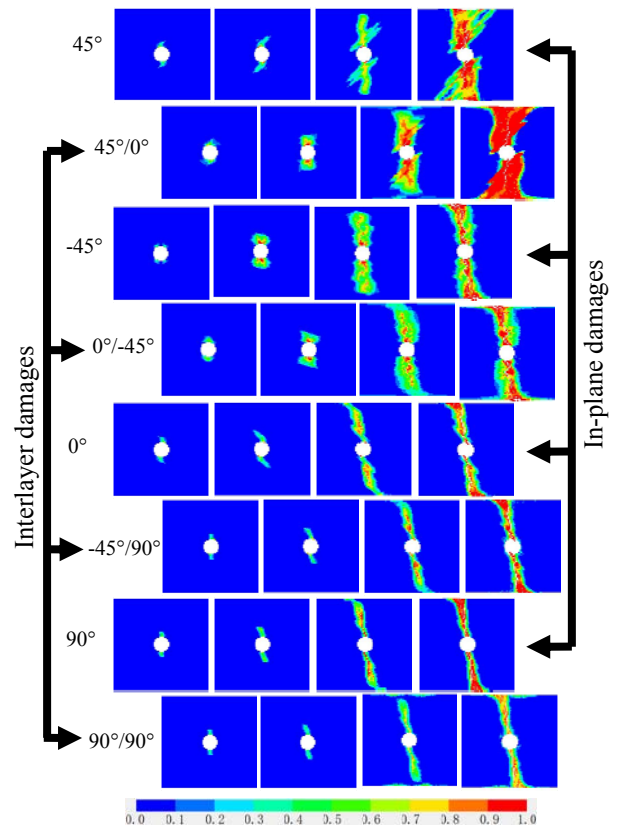
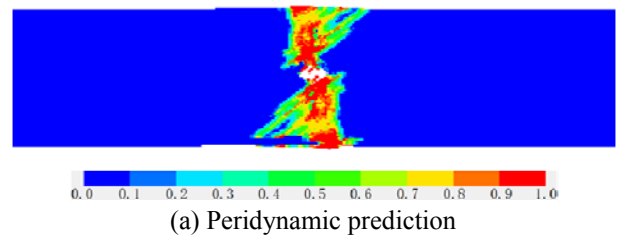


Fig.10 In-plane and interlayer progressive damages in  $[45/0/-45/90]_s$  laminate



(a) Peridynamic prediction



(b) Experiment result

Fig.11 Comparison of final failure modes of peridynamic and experimental results

## References

- [1] K.M. Liew, X. Zhao, A.J.M. Ferreira. A review of meshless methods for laminated and functionally graded plates and shells. *Composite Structures*, 2011, 93(8): 2031-2041.
- [2] V.P. Nguyen, T. Rabczuk, S. Bordas, et al. Meshless methods: A review and computer implementation aspects. *Mathematics and computers in simulation*, 2008, 79(3): 763- 813.
- [3] S.A. Silling. Reformulation of elasticity theory for discontinuities and long-range forces. *Journal of the*

*Mechanics and Physics of Solids*, Vol. 48, No.1: pp 175-209, 2000.

- [4] Sandia National Laboratories. EMU-About EMU. <http://www.sandia.gov/emu/emu.htm>.2011-12-01.
- [5] E. Askari, J.F. Xu, S.A. Silling. Peridynamic analysis of damage and failure in composites. *In: 44th AIAA Aerospace Sciences Meeting and Exhibition*, No.2006-88, Reno, Nevada,2006.
- [6] J.F. Xu, A. Askari, O. Weckner, et al. Peridynamic Analysis of Impact Damage in Composite Laminates. *Journal of Aerospace Engineering*, 2008, 21(3):187-194.
- [7] J.F. Xu, A. Askari, O. Weckner et al. Modeling hail impact damage and residual strength in composite structures. *In: 16th International conference on composite materials*, July 8-13,Kyoto,Japan,2007.
- [8] B. Kilic. Peridynamic theory for progressive failure prediction in homogeneous and heterogeneous materials [PHD Thesis]. Tucson: The University of Arizona, 2008.
- [9] B. Kilic, A. Agwai, E. Madenci. Peridynamic theory for progressive damage prediction in center-cracked composite laminates. *Composite Structures*, 2009, 90(2): 141-151.
- [10] W.K. Hu, Y.D. Ha, F. Bobaru. Peridynamic model for dynamic fracture in unidirectional fiber-reinforced composites. *Computer Methods in Applied Mechanics and Engineering*, 2012, 217- 220:247-261.
- [11] S.A. Silling, E. Askari. A meshfree method based on the peridynamic model of solid mechanics. *Computers and Structures*, 2005, 83(17-18):1526-1535.
- [12] J.D. Owens, M. Houston, D. Luebke, et al. GPU Computing. *Proceedings of the IEEE*, 2008, 96(5): 879-899.
- [13] S. Che, M. Boyer, J.Y. Meng, et al. A performance study of general purpose applications on graphics processors using CUDA. *Journal of Parallel and Distributed Computing*, 2008, 68(10): 1370-1380.
- [14] NVIDIA, CUDA C Programming Guide. [http://developer.download.nvidia.com/compute/DevZone/docs/html/C/doc/CUDA\\_C\\_Programming\\_Guide.pdf](http://developer.download.nvidia.com/compute/DevZone/docs/html/C/doc/CUDA_C_Programming_Guide.pdf). 2012-07-01.
- [15] J. Sanders, E. Kandrot. *Cuda by Example: An Introduction to General-Purpose GPU Programming*. Beijing: Tsinghua University Press, 2010: 37-57.
- [16] Standard Test Method for Open-Hole Tensile Strength of Polymer Matrix Composite Laminates, ASTM D 5766/D5766M-11. American Society for Testing and Materials (ASTM). West Conshohocken, PA, USA.
- [17] E.J. Pineda, A.M. Waas, B.A. Bednarczyk, et al. Progressive damage and failure modeling in notched laminated fiber reinforced composites. *International Journal of Fracture*, Vol.158, No.2: pp125-143, 2009.
- [18] G.H. Staab, A. Gilat. High strain rate response of angle-ply glass/epoxy laminates. *Journal of Composite Materials*, 1995, 29(10): 1308-1320.